Time Dependent Behavior of a Localized Electron at a Heterojunction Boundary of Graphene: Supporting Information

Min Seok Jang,[1, a)] Hyungjun Kim,[2, 3, a)] Harry A. Atwater,[1, b)] and William A. Goddard III[3, c)]

[1)] *Thomas J. Watson Laboratories of Applied Physics, California Institute of Technology, MC 128-95, Pasadena, CA 91125*

[2)] *Materials and Process Simulation Center, Beckman Institute, California Institute of Technology, MC 139-74, Pasadena, CA 91125*

[3)] *Center for Materials Simulations and Design, Graduate School of EEWS, Korea Advanced Institute of Science and Technology, Daejeon 305-701, Republic of Korea*

[a)] Authors with equal contribution

[b)] Electronic mail: haa@caltech.edu

[c)] Electronic mail: wag@wag.caltech.edu

I. TIME UPDATE EQUATIONS FOR GRAFDTD

Neglecting inter-valley scattering, the low energy carrier dynamics of graphene around K point can be described by the 2D massless Dirac Hamiltonian

$$\left[-i\hbar v_F \vec{\sigma} \cdot \vec{\nabla} + U\right] \Psi = i\hbar \frac{\partial \Psi}{\partial t}, \tag{S1}$$

where $\Psi = (\psi_1, \psi_2)$ is a two-component isospinor. v_F denotes the Fermi velocity in graphene, and $U(x, y)$ and $\vec{\sigma} = (\sigma_x, \sigma_y)$ are the external electric potential and the Pauli matrices respectively. Time domain of Eq. (S1) is discretized using velocity Verlet algorithm. The update of ψ_1 and ψ_2 during the time step Δt is carried out via the following three steps:

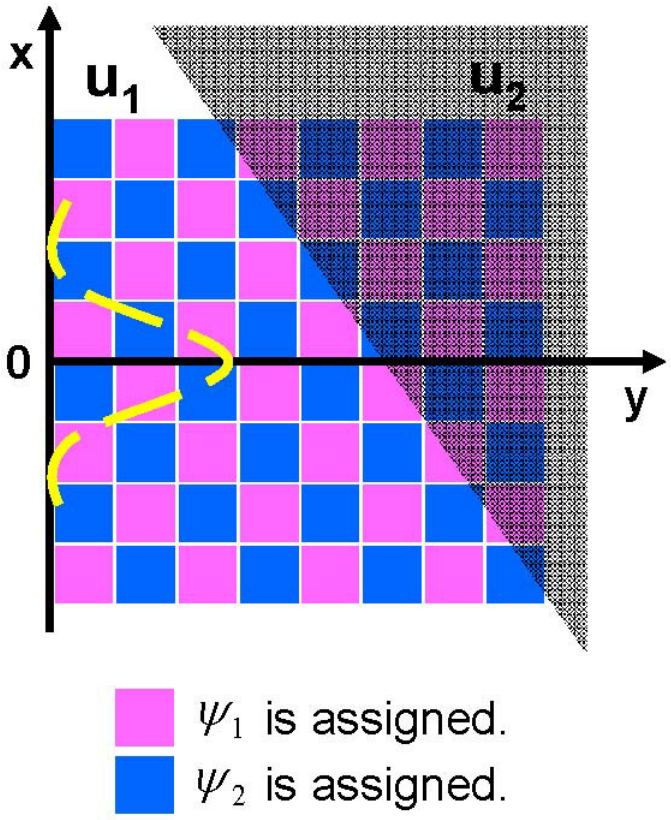

FIG. S1. Schematic diagram of the simulation cell. The graphene is represented as a $(M \times N)$ rectangular grid with the pseudospin components of ψ_1 and ψ_2 alternatively assigned on the grid points due to the symmetric shape of the update scheme. The external potential $U(x, y)$ is applied to represent the different doping levels of Regime 1 and 2. The Gaussian wavepacket is excited from the $y = 0$ boundary, and then propagates along the y-axis.

1. Update of $\psi_1(t+\Delta t/2)$ from $\psi_1(t)$ and $\psi_2(t)$,

$$\psi_1\left(t+\frac{\Delta t}{2}\right)=\left(1-i\frac{V\Delta t}{2\hbar}\right)\psi_1\left(t\right)-\frac{v_F\Delta t}{2}(\partial_x-i\partial_y)\psi_2\left(t\right). \tag{S2}$$

2. Update of $\psi_2(t+\Delta t)$ from $\psi_1(t+\Delta t/2)$ and $\psi_2(t)$,

$$\psi_2\left(t+\Delta t\right)=\frac{1-iV\Delta t/2\hbar}{1+iV\Delta t/2\hbar}\psi_2\left(t\right)-\frac{v_F\Delta t}{1+iV\Delta t/2\hbar}(\partial_x+i\partial_y)\psi_1\left(t+\frac{\Delta t}{2}\right). \tag{S3}$$

3. Update of $\psi_1(t+\Delta t)$ from $\psi_1(t+\Delta t/2)$ and $\psi_2(t+\Delta t)$,

$$\psi_1\left(t+\Delta t\right)=\frac{1}{1+iV\Delta t/2\hbar}\psi_1\left(t+\frac{\Delta t}{2}\right)-\frac{v_F\Delta t/2}{1+iV\Delta t/2\hbar}(\partial_x-i\partial_y)\psi_2\left(t+\Delta t\right). \tag{S4}$$

To treat the spatial derivatives of ψ_1 and ψ_2 numerically, we discretize the two-dimensional space with Δx and Δy, yielding a $(M\times N)$ rectangular grid. Using finite difference method, ∂_x and ∂_y are simply given by

$$\partial_x\psi_a\left(m,n\right)=\frac{\psi_a\left(m+1,n\right)-\psi_a\left(m-1,n\right)}{2\Delta x}, \tag{S5}$$

$$\partial_y\psi_a\left(m,n\right)=\frac{\psi_a(m,n+1)-\psi_a(m,n-1)}{2\Delta y}, \tag{S6}$$

where $a\in 1,2$, and m and n are integer values satisfying $1\leq m\leq M$ and $1\leq n\leq N$. $\psi_a(m,n)$ denotes the value of ψ_a at the spatial grid point of (m,n).

In the implementation of the update scheme, the spatial derivatives of ψ_1 is involved in the update of ψ_2 and that of ψ_2 is involved in the update of ψ_1. Hence, by assigning ψ_1 and ψ_2 on the spatial grid as a checker board pattern as depicted in Fig. S1, we reduce the computational cost by factor of 2.

II. DETAILS ON THE SIMULATION CELLS

The total area of the graphene in the simulations is chosen to be either 2 μm $\times$ 2 μm (when the incident angle, $\theta_I \leq 45°$) or 3 μm $\times$ 3 μm (when $\theta_I > 45°$). The incident angle at the heterojunction interface θ_I is varied from 0° to 80° by 5° increments. The graphene sheet is discretized with $\Delta x = \Delta y = 0.4$ nm, leading to $M = N = 5000$ or $M = N = 7500$ respectively. In order to achieve the maximal numerical stability during the simulation, we chose the time step to be $\Delta t = 0.277$ fs, which satisfies the CFL condition[R. Courant, K. Friedrichs, and H. Lewy, Math. Ann. **100**, 3274 (1928)].

III. EXCITATION OF AN ELECTRONIC GAUSSIAN WAVEPACKET AT THE BOUNDARY

The localized Gaussian wavepacket is generated at $y = 0$ boundary as

$$\Psi(x;t)|_{y=0} = N\begin{pmatrix}1\\ i\end{pmatrix}\exp\left(-\frac{x^2}{4\sigma_x^2} - \frac{t^2}{4\sigma_t^2} + i\frac{E_F}{h}t\right) \tag{S7}$$

where N is the normalization constant, $\sigma_x = 50$ nm and $\sigma_t = 50$ fs. This excitation process leads an isotropic Gaussian wavepacket of 50 nm size.

IV. SIMULATION RESULTS FOR THE LAW OF REFLECTION AND THE SNELL'S LAW

When a de Broglie wave of an electron approaches the heterojunction interface, the electron wavepacket is split into two parts, one transmitted and one reflected. To obtain

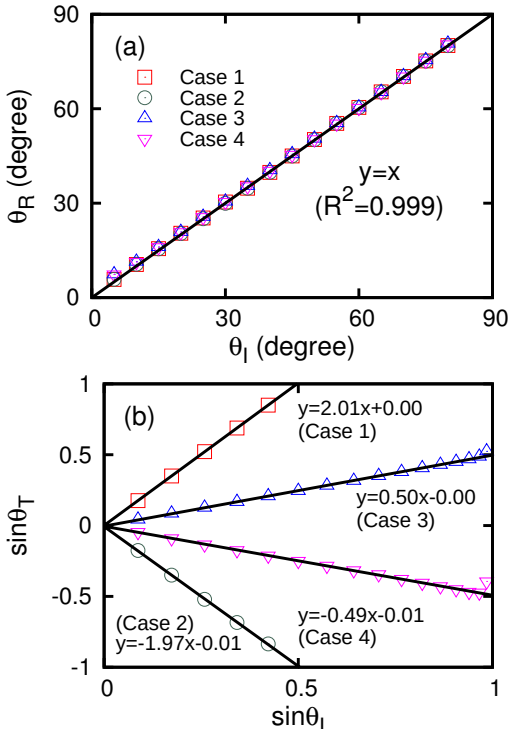

FIG. S2. Demonstration that the Gaussian electron wavepacket obeys the law of reflection and the law of refraction. Part (a) shows the plot of θ_R versus θ_I. Simulation results are shown for all four different cases of These are aligned on top of $y = x$ line ($R^2 = 0.999$), indicating $\theta_I = \theta_R$.

1. red squares; $(u_1, u_2) = (0, 0.5E_F)$ [i.e. $(n_1, n_2) = (1, 0.5)$],
2. green circles; $(u_1, u_2) = (0, 1.5E_F)$ [i.e. $(n_1, n_2) = (1, -0.5)$],
3. blue triangles; $(u_1, u_2) = (0.5E_F, 0)$ [i.e. $(n_1, n_2) = (0.5, 1)$],
4. magenta reverse-triangles; $(u_1, u_2) = (1.5E_F, 0)$ [i.e. $(n_1, n_2) = (-0.5, 1)$].

Part (b) shows plots of $\sin\theta_T$ versus $\sin\theta_I$ for four different cases, each of which shows a linear fit. The data at $\theta_I = 80°$ are excluded from the fitting because of their relatively large errors. The slope of each line is determined by n_1/n_2 which is 2,-2, 0.5, and -0.5 for cases 1, 2, 3, and 4. This is in excellent agreement with the slopes determined from numerical simulations: 2.01, -1.97, 0.50, and -0.49 for the cases 1, 2, 3, and 4, respectively.

the angle of reflection θ_R and refraction θ_T, as a function of the angle of incidence θ_I, we track the position of the wavepacket, $\langle \mathbf{x} \rangle = \int \Psi^\dagger \mathbf{x} \Psi dxdy$. This leads to Fig. S2.(a) for the dependence of θ_R on θ_I. Clearly, all data points lie on the line of $y = x$ ($R^2 = 0.999$), indicating that the law of reflection remains valid in the graphene electron system.

We find that $\sin\theta_T$ depends linearly on $\sin\theta_I$ as shown in Fig. S2.(b). The slopes are 0.50 [case 1: $(u_1, u_2) = (0, 0.5E_F)$], -0.49 [case 2: $(u_1, u_2) = (0, 1.5E_F)$], 2.01 [case 3: $(u_1, u_2) = (0.5E_F, 0)$], and -1.97 [case4: $(u_1, u_2) = (1.5E_F, 0)$]. As θ_I approaches 90°, the electron travels along the direction of the boundary leading to an error due to the finite discretization of the space, preventing a sharp boundary. Thus, we omitted the data at $\theta_I = 80°$ from the fittings.

Using the optical analogy, we expect that the path of the graphene electrons would follow the Snell's law:

$$n_1 \sin\theta_I = n_2 \sin\theta_T. \tag{S8}$$

For graphene we introduce the effective refractive index n_a,

$$n_a = 1 - \frac{u_a}{E_F}, \tag{S9}$$

where $a \in 1, 2$. The definition of Eq. (S9) implies that the cases 1, 2, 3, and 4 are analogous to the cases in which EM waves transmit at a boundary between two media with $(n_1, n_2) = (1, 0.5)$, $(1, -0.5)$, $(0.5, 1.0)$, and $(-0.5, 1.0)$ respectively. This yields n_1/n_2 of 2,-2, 0.5, and -0.5 that correspond to the slopes of Fig. S2.(b) of 2.01, -1.97, 0.50, and -0.49, respectively.

V. KLEIN TUNNELING

Since GraFDTD solves the differential equation based on the grid, the grid size can be affect on the simulation result. In order to eliminate such an artifact in determining the Klein tunneling behavior, we checked the convergence of transmittance, T_{GE} as reducing the grid size, $\Delta x (= \Delta y)$. Fig. (S3) shows the plot of T_{GE} versus $\Delta x^2 (= \Delta y^2)$ for 4 different height of step potentials: $(u_1, u_2) = (0, 1.5E_F)$, $(u_1, u_2) = (0, 2.0E_F)$, $(u_1, u_2) = (0, 2.5E_F)$, and

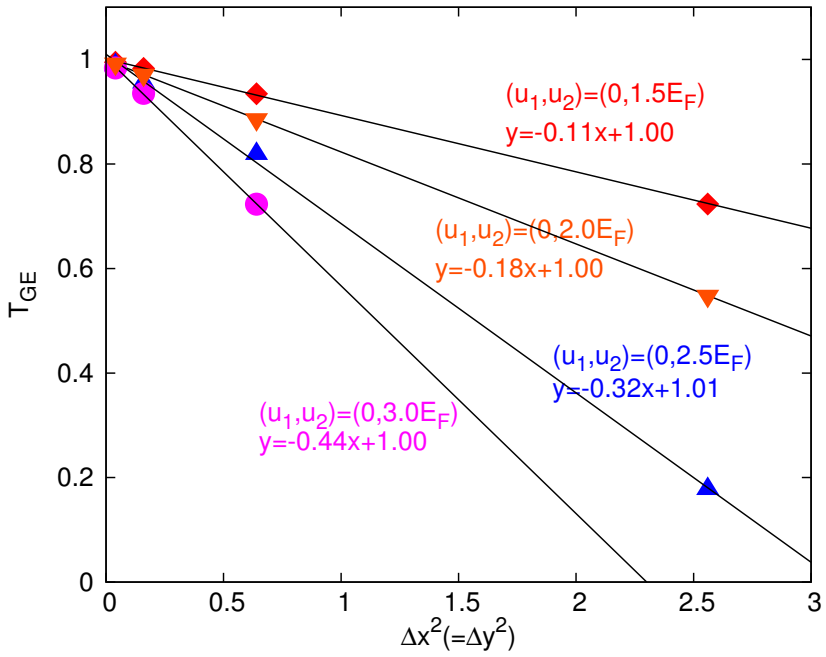

FIG. S3. Transmittance of a graphene electrons (T_{GE}) at the heterojunction boundaries of 4 different heights of

1. red diamonds; $(u_1, u_2) = (0, 0.5E_F)$,
2. orange reverse-triangles; $(u_1, u_2) = (0, 2.0E_F)$,
3. blue triangles; $(u_1, u_2) = (0, 2.5E_F)$,
4. magenta circles; $(u_1, u_2) = (0, 3.0E_F)$.

T_{GE} linearly depends on the grid area Δx^2, which leads the y-intercept of 1.00, 1.00, 1.01, and 1.00 for the cases of 1, 2, 3, and 4, respectively. This concludes that the Klein tunneling occurs for the spatially localized electrons regardless of the potential height. Additionally, this implies that we need a very fine grid for the simulation of extremely abrupt potential profiles in order to avoid any artifact from the finite size of grid.

$(u_1, u_2) = (0, 3.0E_F)$. We figured out that the T_{GE} is linearly dependent on the grid area, and the linear fit leads us to estimate the T_{GE} in the limit of $\Delta x \to 0$. $\lim_{\Delta x \to 0} T_{GE}$ is determined as 1.00, 1.00, 1.01, and 1.00 for four different height of step potentials of $1.5E_F$, $2.0E_F$, $2.5E_F$, and $3.0E_F$, respectively. We conclude that the time-dependent electronic wavepacket exhibits the Klein tunneling behavior regardless of the height of the step potential. However, the numerical error due to the finite size of the grid becomes more significant as the potential becomes more abrupt. Therefore, in order to observe the Klein tunneling in extremely high potential profile, we need to employ a very fine grids.